# Complex Formation between Heptakis(2,6-di-*O*-methyl)-*β*-cyclodextrin and Cyclopentadienyl Molybdenum(II) Dicarbonyl Complexes: Structural Studies and Cytotoxicity Evaluations

Cláudia C. L. Pereira,[†] Cátia V. Diogo,[‡] Ana Burgeiro,[‡] Paulo J. Oliveira,[‡] Maria Paula M. Marques,[§] Susana S. Braga,*[,†] Filipe A. Almeida Paz,[†] Martyn Pillinger,[†] and Isabel S. Gonçalves*[,†]

*Department of Chemistry, CICECO, University of Aveiro, 3810-193 Aveiro, Portugal, Center for Neuroscience and Cell Biology, Department of Zoology, University of Coimbra, 3004-517 Coimbra, Portugal, and Department of Biochemistry, Faculty of Science and Technology, University of Coimbra, Apartado 3126, 3001-401 Coimbra, Portugal*

*Received May 8, 2008*

The inclusion compounds isolated from nonaqueous solutions of heptakis(2,6-di-*O*-methyl)-*β*-cyclodextrin (DIMEB) and the complexes $[CpMoL_2(CO)_2](BF_4)$ (L = MeCN, $L_2$ = 2,2′-biimidazole) were characterized in the solid state by powder X-ray diffraction (XRD), thermogravimetric analysis (TGA), $^{13}C\{^1H\}$ CP/MAS NMR, and FTIR spectroscopy. Powder XRD showed that the compound with $[CpMo(MeCN)_2(CO)_2](BF_4)$ was amorphous, while that with $[CpMo(H_2biim)(CO)_2](BF_4)$ was microcrystalline. The powder XRD pattern of the microcrystalline product could be satisfactorily indexed in the orthorhombic crystal system with space group $P2_12_12_1$ and final unit cell parameters of $a$ = 28.489(3) Å, $b$ = 19.198(2) Å, and $c$ = 16.042(2) Å. A hypothetical structural model for the crystal packing was obtained through Monte Carlo optimizations using fixed DIMEB, $[CpMo(H_2biim)(CO)_2]^+$, and $BF_4^-$ geometries. In the final model the $BF_4^-$ anions are housed inside the toroidal cavity of DIMEB and the organometallic complex cations are regularly distributed in between the DIMEB-tetrafluoroborate complexes, occupying the intermolecular void spaces. The cytotoxicity of the free complexes and the corresponding DIMEB adducts was tested against K1735-M2 mouse melanoma cells and H9c2 rat myoblast cells in aqueous solution. The MeCN complex and its corresponding DIMEB adduct showed no significant activity for use as chemotherapeutic agents. In contrast, the biimidazole complex exhibited significant cytotoxicity against K1735-M2 cells, especially for concentrations above 50 $\mu$M, and the cytotoxicity was even higher when the DIMEB adduct was used. Epifluorescence microscopy indicated that mitochondrial alterations took place at an earlier time point than major changes in cell morphology.

## Introduction

Toward the end of the 1970s, inorganic compounds started to have a tremendous impact on medicine, mainly due to Rosenberg's serendipitous discovery of the potent antitumor activity of cisplatin, a square-planar $Pt^{II}$ complex (*cis*-dichlorodiamineplatinum(II)).[1] Cisplatin continues to be used in 50−70% of all cancer patients, with particular activity against testicular, ovarian, bladder, and neck cancers. The drug does, however, present severe side effects such as nephrotoxicity, neurotoxicity, and emesis, and many human cancers either have a natural resistance to cisplatin or acquire resistance during treatment. In an effort to overcome these problems, modified versions of cisplatin have been studied, such as the second-generation drug carboplatin, which exhibits reduced toxicity, and the third generation drug satraplatin, the first orally bioavailable platinum drug.[2] There has also been a huge effort to develop other metal coordination complexes as antitumor agents.[3] Two ruthenium-based complexes, namely, (ImH)[*trans*-$RuCl_4$(DMSO-$\kappa S$)(Im)] (Im = imidazole, DMSO-$\kappa S$ = S-bonded dimethylsulfoxide) (NAMI-A) and (IndH)[*trans*-$RuCl_4(Ind)_2$] (Ind = indazole) (KP1019), have successfully completed phase 1 clinical trials and are scheduled to enter phase 2 trials in the near future.[4,5]

One of the potential drawbacks of using coordination complexes as antitumor agents is their instability and complicated ligand exchange chemistry. Although some exchange reactions are essential for inducing the appropriate therapeutic properties, others can lead to drug deactivation and detoxification. Accordingly, it has been suggested that organometallic compounds might be better drug candidates because they exhibit slow rates of ligand dissociation in biological systems.[6] The

* To whom correspondence should be addressed. E-mail: igoncalves@ua.pt (I.S.G.); sbraga@ua.pt (S.S.B.).
[†] University of Aveiro.
[‡] Center for Neuroscience and Cell Biology, University of Coimbra.
[§] Department of Biochemistry, University of Coimbra.

(1) Rosenberg, B.; Van Camp, L.; Trosko, J. E.; Mansour, V. H. *Nature* **1969**, *222*, 385.
(2) Fricker, S. P. *Dalton Trans.* **2007**, 4903.
(3) Ott, I.; Gust, R. *Arch. Pharm. Chem. Life Sci.* **2007**, *340*, 117.
(4) Bergamo, A.; Sava, G. *Dalton Trans.* **2007**, 1267.
(5) Ang, W. H.; Dyson, P. J. *Eur. J. Inorg. Chem.* **2006**, 4003.
(6) (a) Yan, Y. K.; Melchart, M.; Habtemariam, A.; Sadler, P. J. *Chem. Commun.* **2005**, 4764. (b) Allardyce, C. S.; Dorcier, A.; Scolaro, C.; Dyson, P. J. *Appl. Organomet. Chem.* **2005**, *19*, 1. (c) Dyson, P. J.; Sava, G. *Dalton Trans.* **2006**, 1929.

10.1021/om800413w CCC: $40.75 
Publication on Web 09/04/2008

**Chart 1**

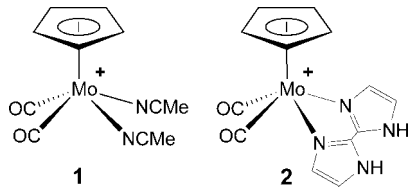


field of organometallic pharmaceuticals is not a new one and dates back to the pioneering work of Köpf and Köpf-Maier, who investigated the antitumor activity of bent metallocene complexes of the type $Cp_2MX_2$ (M = Ti, V, Nb, Mo; e.g., X = Cl, Br, acido ligand).[7] Titanocene dichloride was the first nonplatinum metal complex to enter clinical trials. However, the hydrolytic instability and disappointing phase 2 results of $Cp_2TiCl_2$ have prompted investigators to focus on derivatives of $Cp_2TiCl_2$ and related metallocenes.[8,9] The search for effective organometallic drug candidates has extended to a broad variety of compounds, including, for example, the vectorization of cyclopentadienyl compounds with tamoxifen,[10] and ruthenium(II) arene complexes.[5,6]

The eventual clinical application of metal-based drugs may depend to a large extent on developing methods to safely shepherd the drugs through specific areas of the body. Molecular encapsulation is one approach that has the potential to overcome a number of hurdles, for example poor aqueous solubility and stability and high toxicity. Organic host molecules such as cyclodextrins (CDs) and cucurbiturils have been identified as potentially useful carrier and protecting agents for anticancer complexes,[11,12] with considerable attention being focused on CDs due to their frequent use in drug delivery formulations.[13] CDs are water-soluble cyclic oligosaccharides capable of forming inclusion complexes with a wide range of organic molecules, inorganic ions, and metallo-organic species.[14] Inclusion complexes containing CDs and the anticancer agents carboplatin[11a−c] and $Cp_2MX_2$ (M = Ti, V, Nb, Mo)[11e−i] have already been described. Utsuki et al. reported that interstitial delivery of a carboplatin-HP$\alpha$CD complex from a microencapsulated formulation was effective against an experimental rat glioma model.[15] Cytotoxicity experiments carried out on human adenocarcinoma cells indicated that the antitumor activity of $Cp_2MoCl_2$ can be enhanced by association with cyclodextrins.[16]

We recently described structural studies of inclusion complexes comprising $[CpMoL_2(CO)_2](BF_4)$ (L = MeCN, $L_2$ = 2,2′-biimidazole; Chart 1) encapsulated in $\beta$-CD and heptakis(2,3,6-tri-*O*-methyl)-$\beta$-CD (TRIMEB) hosts.[17] Half-sandwich complexes of molybdenum are worth considering as potential metallopharmaceuticals because they exist in a wide range of oxidation states and are compatible with a large array of ligands.[18] In the present work, we have extended the study to include the modified CD heptakis(2,6-di-*O*-methyl)-$\beta$-CD (DIMEB) as host molecule. The superior solubilizing properties of DIMEB make it an attractive delivery agent for drug molecules.[13,19] The inclusion complexes have been characterized in the solid state by various techniques and screened for their cytotoxicity against two different nonhuman cell lines.

## Results and Discussion

**Preparation of the Inclusion Complexes.** A solution of DIMEB in acetonitrile or dichloromethane was added to solutions of $[CpMo(MeCN)_2(CO)_2](BF_4)$ (**1**) in acetonitrile or $[CpMo(H_2biim)(CO)_2](BF_4)$ (**2**) in dichloromethane, and the resultant mixtures were heated at 40 °C for 2 h. A host:guest molar ratio of 1:1 was used for both systems. After evaporation of the solvents under reduced pressure, the products referred to as **1**@DIMEB and **2**@DIMEB were obtained as light red and light brown solids, respectively.

**Powder Diffraction and *ab Initio* Structural Modeling.** When a crystalline phase is obtained, powder X-ray diffraction allows the identification of true inclusion complexes of cyclodextrins, mainly based on the empirical evidence that the powder XRD patterns of these compounds should be clearly distinct from those obtained by the superimposition of the diffractograms for each individual component.[20] However, we were able to isolate the adduct **2**@DIMEB only as a crystalline phase; the adduct **1**@DIMEB, in spite of several efforts at recrystallization, always formed an amorphous phase. Still, this is a good early indication of the stability of **1**@DIMEB, as there was no separation of its components in any of these experiments.

Structural investigations of the crystal packing fashion of **2**@DIMEB from powder X-ray data were performed using the systematic experimental considerations previously described for

(7) (a) Köpf-Maier, P.; Köpf, H. *Chem. Rev.* **1987**, *87*, 1137. (b) Köpf-Maier, P. *Eur. J. Clin. Pharmacol* **1994**, *47*, 1.

(8) (a) Kröger, N.; Kleeberg, U. R.; Mross, K.; Edler, L.; Hossfeld, D. K. *Onkologie* **2000**, *23*, 60. (b) Mross, K.; Robben-Bathe, P.; Edler, L.; Baumgart, J.; Berdel, W. E.; Fiebig, H.; Unger, C. *Onkologie* **2000**, *23*, 576.

(9) (a) Caruso, F.; Rossi, M. *Mini-Rev. Med. Chem.* **2004**, *4*, 49. (b) Causey, P. W.; Baird, M. C.; Cole, S. P. C. *Organometallics* **2004**, *23*, 4486. (c) Abeysinghe, P. M.; Harding, M. M. *Dalton Trans.* **2007**, 3474. (d) Waern, J. B.; Turner, P.; Harding, M. M. *Organometallics* **2006**, *25*, 3417. (e) Vinklárek, J.; Paláčková, H.; Honzíček, J.; Holubová, J.; Holčapek, M.; Císařová, I. *Inorg. Chem.* **2006**, *45*, 2156. (f) Harding, M. M.; Prodigalidad, M.; Lynch, M. J. *J. Med. Chem.* **1996**, *39*, 5012.

(10) (a) Vessières, A.; Top, S.; Beck, W.; Hillard, E.; Jaouen, G. *Dalton Trans.* **2006**, 529. (b) Nguyen, A.; Marsaud, V.; Bouclier, C.; Top, S.; Vessieres, A.; Pigeon, P.; Gref, R.; Legrand, P.; Jaouen, G.; Renoir, J.-M. *Int. J. Pharm.* **2008**, *347*, 128.

(11) (a) Alston, D. R.; Lilley, T. H.; Stoddart, J. F. *J. Chem. Soc., Chem. Commun.* **1985**, 1600. (b) Alston, D. R.; Slawin, A. M. Z.; Stoddart, J. F.; Williams, D. J. *J. Chem. Soc., Chem. Commun.* **1985**, 1602. (c) Alston, D. R.; Ashton, P. R.; Lilley, T. H.; Stoddart, J. F.; Zarzycki, R.; Slawin, A. M. Z.; Williams, D. J. *Carbohydr. Res.* **1989**, *192*, 259. (d) Horvath, G.; Premkumar, T.; Boztas, A.; Lee, E.; Jon, S.; Geckeler, K. E. *Mol. Pharm.* **2008**, *5*, 358. (e) Turel, I.; Demšar, A.; Košmrlj, J. *J. Inclusion Phenom. Macrocyclic Chem.* **1999**, *35*, 595. (f) Vinklárek, J.; Honzíček, J.; Holubová, J. *Central Eur. J. Chem* **2005**, *3*, 72. (g) Pereira, C. C. L.; Nolasco, M.; Braga, S. S.; Paz, F. A. A.; Ribeiro-Claro, P.; Pillinger, M.; Gonçalves, I. S. *Organometallics* **2007**, *26*, 4220. (h) Morales, A.; Struppe, J.; Meléndez, E. *J. Inclusion Phenom. Macrocyclic Chem.* **2008**, *60*, 263. (i) Braga, S. S.; Gonçalves, I. S.; Pillinger, M.; Ribeiro-Claro, P.; Teixeira-Dias, J. J. C. *J. Organomet. Chem.* **2001**, *632*, 11.

(12) (a) Wheate, N. J.; Buck, D. P.; Day, A. I.; Collins, J. G. *Dalton Trans.* **2006**, 451. (b) Buck, D. P.; Abeysinghe, P. M.; Cullinane, C.; Day, A. I.; Collins, J. G.; Harding, M. M. *Dalton Trans.* **2008**, 2328.

(13) (a) Singh, M.; Sharma, R.; Banerjee, U. C. *Biotechnol. Adv.* **2002**, *20*, 341. (b) Davis, M. E.; Brewster, M. E. *Nat. Rev. Drug Discovery* **2004**, *3*, 1023. (c) Challa, R.; Ahuja, A.; Ali, J.; Khar, R. K. *AAPS PharmSciTech* **2005**, *6*, E329. (d) Uekama, K.; Hirayama, F.; Arima, H. *J. Inclusion Phenom. Macrocyclic Chem.* **2006**, *56*, 3.

(14) Hapiot, F.; Tilloy, S.; Monflier, E. *Chem. Rev.* **2006**, *106*, 767.

(15) Utsuki, T.; Brem, H.; Pitha, J.; Loftsson, T.; Kristmundsdottir, T.; Tyler, B. M.; Olivi, A. *J. Controlled Release* **1996**, *40*, 251.

(16) Braga, S. S.; Marques, M. P. M.; Sousa, J. B.; Pillinger, M.; Teixeira-Dias, J. J. C.; Gonçalves, I. S. *J. Organomet. Chem.* **2005**, *690*, 2905.

(17) Pereira, C. C. L.; Braga, S. S.; Paz, F. A. A.; Pillinger, M.; Klinowski, J.; Gonçalves, I. S. *Eur. J. Inorg. Chem.* **2006**, 4278.

(18) Norton de Matos, M. R. P., Romão, C. C.; Pereira, C. C. L.; Rodrigues, S. S.; Mora, M.; Silva, M. J. P.; Alves, P. M.; Reis, C. A. Compositions comprising organometallic molybdenum compounds for treating cancer. International Patent WO/2005/087783.

(19) Szejtli, J. *J. Inclusion Phenom. Macrocyclic Chem.* **1992**, *14*, 25.

(20) Saenger, W. *Angew. Chem., Int. Ed. Engl.* **1980**, *19*, 344.

other inclusion complexes of cyclodextrins,[11g,21] in particular for $Cp_2NbCl_2$@TRIMEB[11g] and $CpMo(CO)_3Cl$@TRIMEB.[21a] Crystalline CD inclusion complexes can generally be grouped into distinct isostructural series according to the type of crystal packing arrangement.[22] Within an isostructural series, the gross features of the powder XRD patterns are constant, regardless of the nature of the included guest. To the best of our knowledge, there are no reports in the literature of true host−guest systems in which DIMEB molecules encapsulate organometallic complexes. Indeed, a search of the Cambridge Structural Database[23] (CSD, Version 5.28, three updates, November 2007) revealed only structures with organic guest molecules.[24] A preliminary comparison of the powder XRD pattern of **2**@DIMEB with those of complexes with DIMEB and organic guests indicated the presence of a host−guest system. Of all the DIMEB structures reported to date,[24] only two crystallize in the monoclinic $P2_1$ space group (CSD refcodes QAZYIZ and SAJPOI).[24d] Thus, following the isostructurality concepts developed by Caira,[22] **2**@DIMEB would most likely crystallize in the orthorhombic crystal system with space group $P2_12_12_1$.

The experimental powder XRD pattern of **2**@DIMEB exhibits several features typical of powdered cyclodextrin inclusion compounds, in particular a significant reduction in overall crystallinity compared with pure DIMEB (driven by the inherent structural disorder associated with the host−guest system and the water molecules of crystallization, affected by thermal disorder and housed in the empty voids), poorly resolved reflections at low angle, a significant background up to ca. 30° $2\theta$, and the absence of discernible reflections from the background at higher angles. Nevertheless, by selecting the first 15 more intense and well-resolved reflections, located using the derivative-based peak search algorithm in Fullprof.2k,[25] the powder pattern could be indexed using DICVOL04,[26] for which a fixed absolute error on each line of 0.03° $2\theta$ was employed and no impurity lines were allowed. Initial unit cell metrics in the orthorhombic crystal system were calculated with reasonable figures-of-merit: $M(15)^{27a} = 14.8$ and $F(15)^{27b} = 41.5$. Systematic absences were examined using the software package CHECKCELL,[28] which unambiguously confirmed the space group $P2_12_12_1$ as the most suitable to describe the overall symmetry of the compound. A Le Bail[29] whole-powder-diffraction-pattern profile decomposition using fixed (and manually selected) background points produced a reasonable fitting ($R_{Bragg} = 0.36\%$ and $\chi^2 = 10.7$; see Figure S1 in the Supporting Information) with the unit cell parameters converging to $a =$ 28.489(3) Å, $b =$ 19.198(2) Å, and $c =$ 16.042(2) Å.

The crystal structure modeling and the final selection of a chemically feasible hypothetical packing for **2**@DIMEB using the software package FOX[30] assumed *a priori* that (1) due to electrostatic interactions, the $[CpMo(H_2biim)(CO)_2]^+$ cation and the charge-balancing $BF_4^-$ anion should be in close proximity; (2) individual chemical moieties are distributed in order to effectively fill the available space; (3) interactions between guest molecules and the host DIMEB are essentially of relatively weak nature, being a combination of hydrogen bonds and van der Waals interactions; (4) the overall diffraction of the material is mainly due to the large chemical moieties, and the omission of individual water molecules from the initial model for Monte Carlo optimization will not have a significant impact on the final result; and (5) the molecular geometry of each chemical moiety remains relatively unchanged after inclusion. This latter assumption is critical because a crystal structure of a DIMEB inclusion compound with an organometallic complex is not available in the literature. Consequently, it is necessary to select a conformation for DIMEB from one of the known compounds and assume that it will not be very different from that adopted in a true inclusion compound with an organometallic guest.

The molecular geometrical parameters of the $[CpMo(H_2biim)(CO)_2]^+$ cation and the $BF_4^-$ anion were extracted from the reported crystal structure,[17] with the central molybdenum and boron atoms being taken as the pivot atoms of the corresponding Fenske−Hall *Z*-matrices created using BABEL (hydrogen atoms were removed to simplify the calculations).[31] This strategy facilitates the mobility of these chemical entities (treated as rigid bodies) inside the unit cell boundaries during the global optimization processes. For DIMEB, several different conformations reported in the literature, each exhibiting distinct elliptical distortions of the toroidal cavity, were used, all of them invariably leading to approximately the same final result. For the structural model described here, we selected the DIMEB geometry of the compound reported by Selkti et al. (CSD refcode NITSIS)[32] since it minimizes the number of overlapping neighboring atoms between adjacent moieties.

Monte Carlo optimizations using the optimized parallel tempering algorithm were launched in FOX[30] with the three individual mathematical objects having the parameters of the *Z*-matrices fixed (i.e., each entity was treated as a rigid body). Since the experimental data were collected in an instrument with a Bragg−Brentano geometry and the crystal habit of cyclodextrin compounds is usually plate-like, the powder XRD pattern was assumed *a priori* to be affected by textural effects such as preferred orientation, and a refineable March−Dollase correction[33] was included in the optimization. Antibump restraints and water molecules of crystallization were omitted from the

(21) (a) Braga, S. S.; Paz, F. A. A.; Pillinger, M.; Seixas, J. D.; Romão, C. C.; Gonçalves, I. S. *Eur. J. Inorg. Chem.* **2006**, 1662. (b) Fernandes, J. A.; Lima, S.; Braga, S. S.; Ribeiro-Claro, P.; Rodriguez-Borges, J. E.; Teixeira, C.; Pillinger, M.; Teixeira-Dias, J. J. C.; Goncalves, I. S. *J. Organomet. Chem.* **2005**, *690*, 4801. (c) Petrovski, Z.; Braga, S. S.; Santos, A. M.; Rodrigues, S. S.; Gonçalves, I. S.; Pillinger, M.; Kühn, F. E.; Romão, C. C. *Inorg. Chim. Acta* **2005**, *358*, 981.

(22) Caira, M. R. *Rev. Roumaine Chim.* **2001**, *46*, 371.

(23) (a) Allen, F. H. *Acta Crystallogr., Sect. B: Struct. Sci.* **2002**, *58*, 380. (b) Allen, F. H.; Motherwell, W. D. S. *Acta Crystallogr., Sect. B: Struct. Sci.* **2002**, *58*, 407.

(24) DIMEB inclusion compounds have the CSD refcodes BOYGAX, COFLOY, DEZMIE10, DEZMOK10, NITSIS, PABNEM, QAZYEV, QAZYIZ, SAJPOI, WAGHAN01, and YAPSEN10 and can be found in the following references:(a) Tsorteki, F.; Mentzafos, D. *Carbohydr. Res.* **2002**, *337*, 1229. (b) Harata, K. *Chem. Commun.* **1999**, 191. (c) Armspach, D.; Ashton, P. R.; Ballardini, R.; Balzani, V.; Godi, A.; Moore, C. P.; Prodi, L.; Spencer, N.; Stoddart, J. F.; Tolley, M. S.; Wear, T. J.; Williams, D. J. *Chem.−Eur. J.* **1995**, *1*, 33. (d) Harata, K.; Hirayama, F.; Uekama, K.; Tsoucaris, G. *Chem. Lett.* **1988**, 1585. (e) Harata, K. *Bull. Chem. Soc. Jpn.* **1988**, *61*, 1939. (f) Pohlmann, H.; Gdaniec, M.; Eckle, E.; Geiger, G.; Stezowski, J. J. *Acta Crystallogr., Sect. A: Found. Crystallogr.* **1984**, *40*, C276.

(25) (a) Rodriguez-Carvajal, J. FULLPROF−A Program for Rietveld Refinement and Pattern Matching Analysis. *Abstract of the Satellite Meeting on Powder Diffraction of the XV Congress of the IUCR*; Toulouse, France, 1990; p 127. (b) Roisnel, T., Rodriguez-Carvajal, J. WinPLOTR [June 2005]−A Windows Tool for Powder Diffraction Pattern Analysis. *Proceedings of the Seventh European Powder Diffraction Conference (EPDIC 7), Mater. Sci. Forum*; 2001; Vols. *378−381*, pp 118−123.

(26) Boultif, A.; Louer, D. *J. Appl. Crystallogr.* **2004**, *37*, 724.

(27) (a) Boultif, A.; Louer, D. *J. Appl. Crystallogr.* **1991**, *24*, 987. (b) Louer, D. In *Automatic Indexing: Procedures and Applications, Accuracy in Powder Diffraction II*; Gaithersburg, MD, 1992; pp 92−104.

(28) Laugier, J., Bochu, B. *CHECKCELL−A Software Performing Automatic Cell/Space Group Determination*; Collaborative Computational Project Number 14 (CCP14); Laboratoire des Matériaux et du Génie Physique de l'Ecole Supérieure de Physique de Grenoble (INPG): France, 2000.

(29) LeBail, A.; Duroy, H.; Fourquet, J. L. *Mater. Res. Bull.* **1988**, *23*, 447.

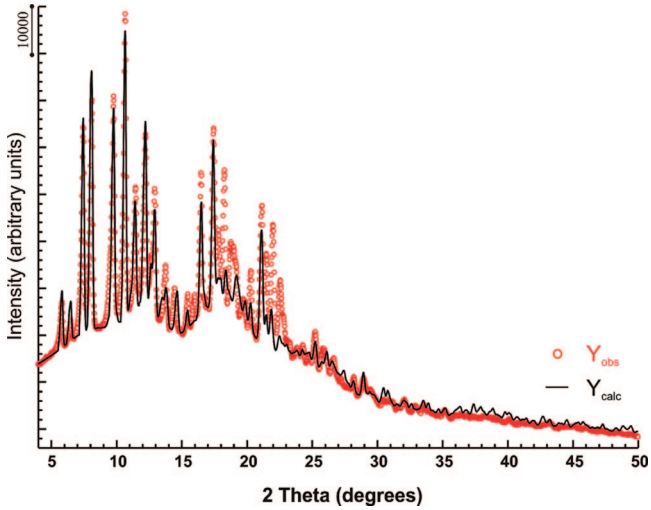


**Figure 1.** Experimental (red circles) and FOX-simulated (solid black line) powder XRD patterns of **2**@DIMEB.

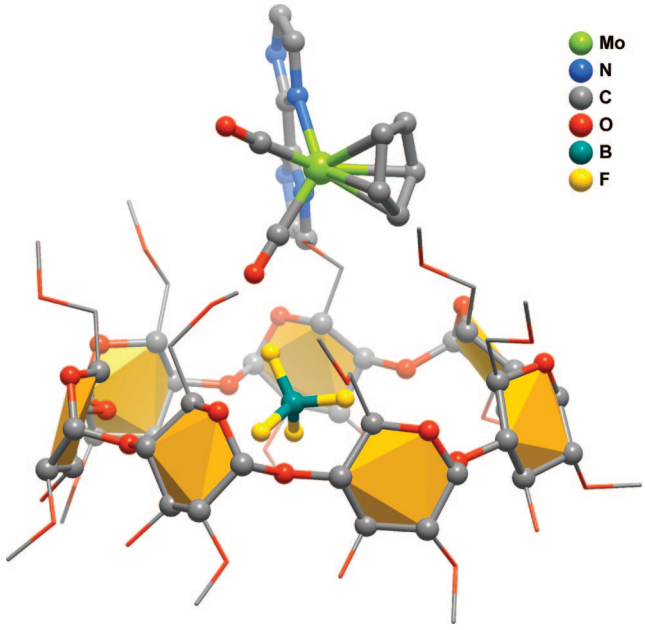


**Figure 2.** Schematic representation of the individual chemical moieties that make up the asymmetric unit of the hypothetical structural model of **2**@DIMEB. The pendant groups attached to the seven α-D-glucopyranoside units of DIMEB are drawn in stick mode and represent (especially $-CH_2OCH_3$ and $-OCH_3$) the moieties that were susceptible to rotation (to avoid structural overlap) during unrestrained refinement using FOX.

structural model. Several optimizations were launched at the same time, all starting from distinct random crystallographic positions for the three chemical moieties. All models converged to nearly the same spatial distribution of the host and guest molecules with comparable *R* factors.

After full convergence of the Monte Carlo optimization (approximately three full days of computation), the permutation in $P2_12_12_1$ of the three chemical entities produced a structural model whose simulated powder pattern compares well with the experimental one, with a calculated weighted residual of $R_{wp} = 0.102$ (Figure 1). Fractional atomic coordinates and a CIF file for the hypothetical structural model are supplied as Supporting Information. Remarkably, these structural studies clearly demonstrate that in **2**@DIMEB the chemical moiety housed inside the toroidal cavity of DIMEB is the $BF_4^-$ anion instead of the expected cationic organometallic complex (Figure 2). However, the two charged species are still in close proximity, with a Mo···B distance of ca. 5.96 Å, which is slightly longer than the analogous value of ca. 5.05 Å found in the crystal structure of $[CpMo(H_2biim)(CO)_2](BF_4)$ (**2**),[17] most likely due to the presence of the bulky DIMEB molecule. In the structural model of **2**@DIMEB, the cations are regularly distributed in between the DIMEB hosts, occupying the intermolecular void spaces (Figures 3 and 4). This unusual structural feature is not unprecedented and was previously reported by K. Harata for the DIMEB complexes with *p*-iodophenol and *p*-nitrophenol.[24e]

**Thermal Behavior.** Figure 5 compares the TGA curves of **1**@DIMEB and **2**@DIMEB with those of DIMEB and 1:1 physical mixtures of DIMEB and either complex **1** or **2**. DIMEB decomposes abruptly in the temperature range 325−410 °C with a mass loss of 87%, followed by a smoother loss of 8% up to 600 °C. In the physical mixture of DIMEB and complex **1**, prepared by grinding the two components together at room temperature, the well-defined step centered around 150 °C (ca. 5% mass loss) corresponds to the removal of the acetonitrile and CO ligands from the complex,[17] and DIMEB decomposition is shifted by about 40 °C to lower temperature compared with the pure CD. The lower thermal stability of the cyclodextrin in the physical mixture is probably induced by the second-stage decomposition of the organometallic complex, which extends from about 250 to 500 °C and involves the decomposition of the cyclopentadienyl group and the tetrafluoroborate counterion.[17] Compound **1**@DIMEB exhibits a somewhat different TG behavior. After removal of water molecules from room temperature to ca. 80 °C (3.7% mass loss), the initial fragmentation of the complex appears as a broad step centered around 150 °C, and the organic macrocycle begins to decompose at about 240 °C, compared with 300 °C for the physical mixture (and 340 °C for pure DIMEB). The temperature of 240 °C roughly corresponds to the point where the second-stage decomposition of complex **1** begins, indicating that the three components, DIMEB, $[CpMo(MeCN)_2(CO)_2]^+$, and $BF_4^-$, are in intimate contact in **1**@DIMEB. Comparable results were obtained with **2**@DIMEB (Figure 5), the main difference being that no obvious step is present for the decomposition of the organometallic complex because the pure complex **2** decomposes in a series of overlapping steps that extend from room temperature to 475 °C.[17]

**Spectroscopic Characterization.** The $^{13}C\{^1H\}$ CP/MAS NMR spectra of DIMEB, **1**@DIMEB, and **2**@DIMEB are shown in Figure 6. The spectrum for DIMEB is in agreement with that reported by Takashimi et al.[34] and can be assigned on the basis of the well-known spectra for unmodified β-CD and permethylated β-CD (TRIMEB).[11g] In the spectra of **1**@DIMEB and **2**@DIMEB, the signals for the cyclodextrin carbon atoms are slightly broader than those of pure DIMEB, which could be due to differences in crystallinity (especially for **1**@DIMEB) and/or a change in the structure of DIMEB to a more

(30) (a) Favre-Nicolin, V.; Cerný, R. *J. Appl. Crystallogr.* **2002**, *35*, 734. (b) Favre-Nicolin, V., Cerný, R. *FOX−A Program for ab Initio Structure Solution from Powder Diffraction Data*; Program Developed for the Swiss National Science Foundation; University of Geneva: Geneva, Switzerland, 2000.

(31) Walters, P.; Stahl, M. *BABEL Version 1.3−A Program for the Interconversion of File Formats Used in Molecular Modelling*; Department of Chemistry, University of Arizona: Tucson, AZ, 1996.

(32) Selkti, M.; Navaza, A.; Villain, F.; Charpin, P.; De Rango, C. *J. Inclusion Phenom. Macrocyclic Chem.* **1997**, *27*, 1.

(33) (a) March, A. *Z. Kristallogr.* **1932**, *81*, 285. (b) Dollase, W. A. *J. Appl. Crystallogr.* **1986**, *19*, 267.

(34) Takashimi, Y.; Sakamoto, K.; Oizumi, Y.; Yamaguchi, H.; Kamitori, S.; Harada, A. *J. Inclusion Phenom. Macrocyclic Chem.* **2006**, *56*, 45.

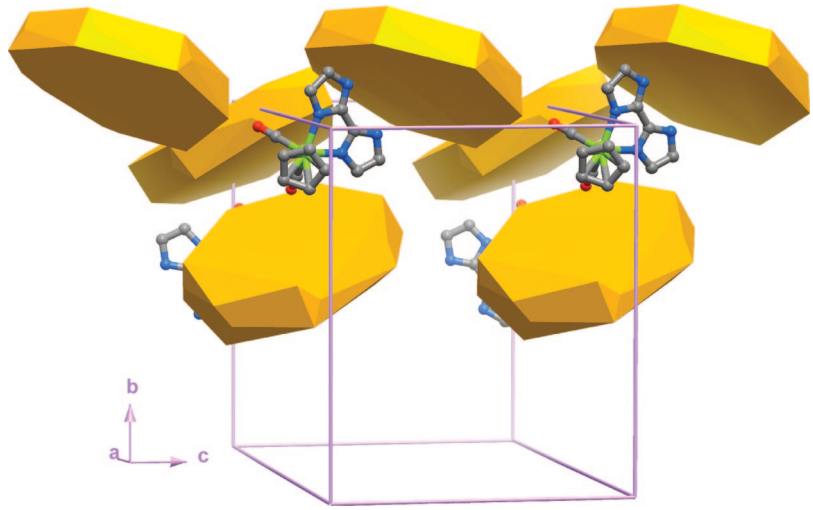


**Figure 3.** Schematic representation of the distribution of DIMEB molecules (represented as large seven-faced polyhedrons) and $[CpMo(H_2biim)(CO)_2]^+$ cations (drawn in ball-and-stick mode) along the [001] direction of the unit cell in **2**@DIMEB, emphasizing how the organometallic complexes are located in the intermolecular spaces rather than within the host cavities. $BF_4^-$ anions are omitted for clarity.

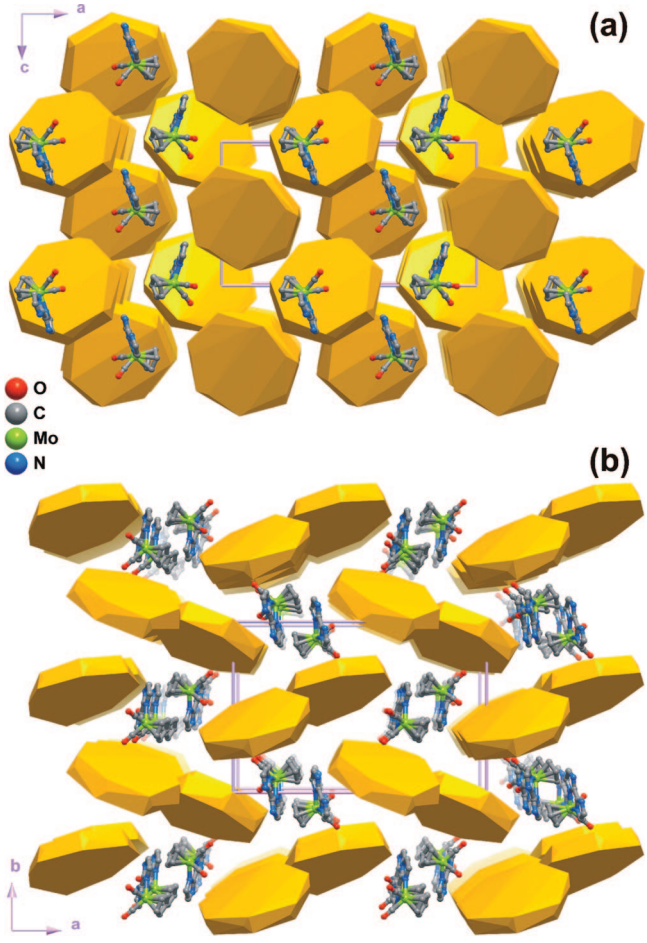


**Figure 4.** Crystal packing of **2**@DIMEB viewed in perspective along the [010] (a) and [001] (b) directions of the unit cell. See the caption to Figure 3 for further details.

symmetrical one as a result of complexation with a guest species.[11g,17,21a,34] The $^{13}C\{^1H\}$ CP/MAS NMR spectrum of **2**@DIMEB shows additional signals at 96.9 (Cp), 122.5 and 134.7 ($H_2$biim) for the molybdenum-coordinated ligands, which are essentially unshifted compared with the corresponding signals for the free complex **2**.[17] No Cp resonance could be observed for **1**@DIMEB due to overlap with the broad C1 signal

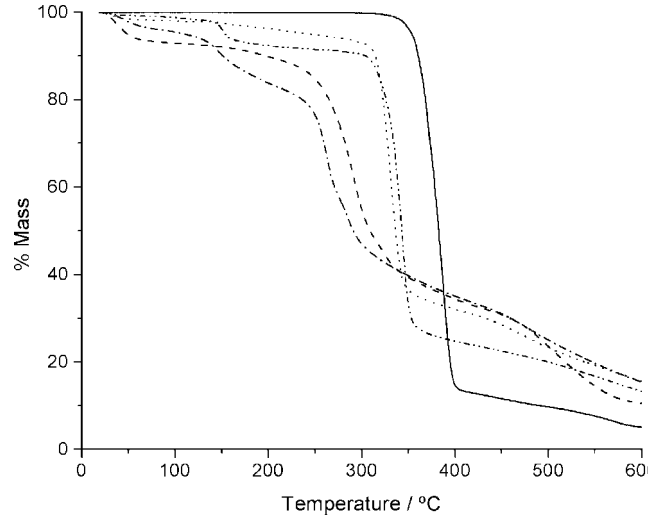


**Figure 5.** Thermogravimetric analysis profiles of DIMEB (—), the 1:1 physical mixture of DIMEB and $[CpMo(MeCN)_2(CO)_2](BF_4)$ (**1**) (- • • - • •), **1**@DIMEB (- • - •), the 1:1 physical mixture of DIMEB and $[CpMo(H_2biim)(CO)_2](BF_4)$ (**2**) (• • •), and **2**@-DIMEB (- - -).

of DIMEB. For both inclusion compounds it was not possible to clearly identify the resonances (masked in the background) of the molybdenum-coordinated CO groups, even when contact times of 2 ms were used. The presence of these groups was confirmed by IR spectroscopy. Thus, in addition to the intense and typical bands of the cyclodextrin host, the spectra contained two bands in the CO stretching region (1890−1990 $cm^{-1}$), as expected for a complex of the type $[CpMoL_2(CO)_2]^+$. The high-frequency band for both compounds was unshifted compared with the corresponding band for the free complex, while the second band at lower frequency was blue-shifted by about 12 $cm^{-1}$. The presence of tetrafluoroborate anions in **1**@DIMEB and **2**@DIMEB was confirmed by the strong $\nu_{BF}$ absorption band at 1087 $cm^{-1}$.

**Cytotoxicity Studies.** Two different nonhuman cell lines were used to investigate the cytotoxicity of the four compounds under study. K1735-M2 cells are a highly invasive melanoma mouse

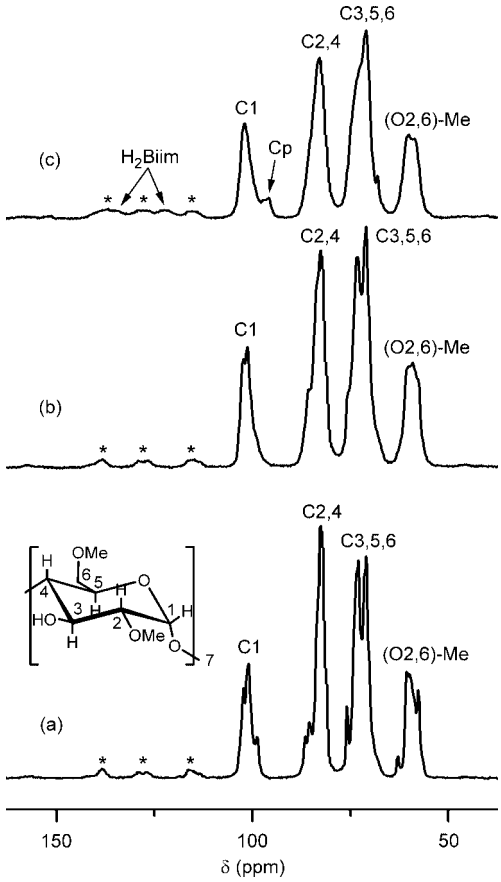


**Figure 6.** $^{13}C\{^{1}H\}$ CP/MAS NMR spectra of DIMEB (a), **1**@DIMEB (b), and **2**@DIMEB (c). Spinning side bands are denoted by asterisks.

cell line,[35] which was previously used to investigate the chemotherapeutic potential of several molecules, including the alkaloid berberine.[36,37] H9c2 is a nontumor rat myoblast cell line and has been extensively used to investigate the muscle toxicity of novel and clinically used chemotherapeutics.[38,39]

Regarding the melanoma cell line, complex **2** has a higher effect than complex **1**, particularly at the highest concentration of 100 $\mu$M (Figure 7, left-hand column). Like complex **1**, the adduct **1**@DIMEB had no cytotoxic effect at all, showing that DIMEB *per se* does not cause cytotoxic inhibition of cell proliferation. On the other hand, the adduct **2**@DIMEB was superior to complex **2** in terms of inhibition of K1735-M2 cell proliferation, especially again at the highest concentration used. At this concentration, the cytotoxicity of **2**@DIMEB was apparent at an early time point, with a clear inhibitory effect after 24 h, while the free complex **2** exhibits a noticeable inhibition (compared to the control group) only after 48 h.

When investigating the behavior of the compounds toward the H9c2 myoblastic line (Figure 7, right-hand column), the higher effect of complex **2** when compared with **1** was again noticeable, and interestingly some concentrations of **1** (especially 10 $\mu$M) actually increased cell proliferation. An increase in cell proliferation was also observed for some concentrations of **1**@DIMEB, in particular 1 $\mu$M (72 h) and 25 $\mu$M (96 h). The same compound exhibited cytotoxicity when used at the highest concentration (100 $\mu$M), causing inhibition of cell proliferation for 48 and 96 h. Regarding the inclusion compound **2**@DIMEB, some inhibition of myoblast proliferation was observed, although the relative effect (when using 100 $\mu$M) was lower compared with the results for the K1735-M2 cells.

In order to obtain preliminary data on the possible mechanism of cytotoxicity of **2**@DIMEB toward the melanoma cell line, we performed epifluorescence microscopy and investigated whether early nuclear or mitochondrial alterations due to drug treatment could be detected (Figure 8). Three different fluorescent probes were used. TMRM is a cationic probe that has a red fluorescence once accumulated by functional mitochondria. When the organelle is damaged by a foreign compound and loses its transmembrane electric potential (negative inside), the red fluorescence decays. Hoechst 33342 is a probe that binds to DNA. Condensed chromatin due to apoptotic cell death can be visualized due to nuclear shrinkage and increased fluorescence of the probe. Finally, calcein-AM is a probe for cell viability. When cells are viable, and hence with intact plasma membranes, the probe is accumulated inside cells and possesses green fluorescence. When the membrane is disrupted due to necrotic cell death, the green fluorescence is lost.

Time points of 24 and 72 h were analyzed. Regarding the early time point and at the lower concentrations (25 $\mu$M), no alterations were observed in the mitochondrial network or in nuclear organization. Differences were visible at a concentration of 50 $\mu$M, where mitochondrial fragmentation was observed. The alteration preceded the loss of TMRM fluorescence at the highest concentration, indicative of complete mitochondrial depolarization. Nevertheless, despite mitochondrial depolarization, cells remained viable, as noticed by the retention of cytosolic calcein (green fluorescence). In accordance with the cytotoxicity studies, a marked decrease in the number of cells was observed at the higher concentrations tested. After 72 h, the most noticeable effect was a decrease in the number of cells and widespread necrotic phenotype (loss of TMRM and calcein fluorescence) at the highest concentration as well as mitochondrial fragmentation and depolarization in cells with intact plasma membranes.

## Conclusions

This study was motivated by the potential application of half-sandwich complexes of molybdenum as anticancer agents. The complexes with the general formula $[CpMoL_2(CO)_2](A)$ are an interesting starting point because they represent a relatively large family of molybdenum(II) derivatives and are compatible with a broad spectrum of ancillary ligands. In testing the complexes $[CpMo(MeCN)_2(CO)_2](BF_4)$ (**1**) and $[CpMo(H_2biim)(CO)_2](BF_4)$ (**2**) against two different cell lines, each one being an established model for cytotoxicity analyses, dissimilar results were obtained. Complex **1** and the adduct **1**@DIMEB showed no significant activity for use as chemotherapeutic agents. Regarding the myoblastic H9c2 cell lines, cell proliferation actually increased for some concentrations. The biimidazole derivative **2** exhibited significant cytotoxicity against the K1735-M2 cell line, especially at the highest concentrations used. However, no selectivity was observed since **2** was also toxic for the myoblast cell line. Even higher cytotoxicity against K1735-M2 cells was observed when the adduct **2**@DIMEB was

(35) Repesh, L. A. *Invasion Metastasis* **1989**, *9*, 192.
(36) Pereira, G. C.; Branco, A. F.; Matos, J. A.; Pereira, S. L.; Parke, D.; Perkins, E. L.; Serafim, T. L.; Sardão, V. A.; Santos, M. S.; Moreno, A. J.; Holy, J.; Oliveira, P. J. *J. Pharmacol. Exp. Ther.* **2007**, *323*, 636.
(37) Serafim, T. L.; Oliveira, P. J.; Sardão, V. A.; Perkins, E.; Parke, D.; Holy, J. *Cancer Chemother. Pharmacol.* **2008**, *61*, 1007.
(38) Turakhia, S.; Venkatakrishnan, C. D.; Dunsmore, K.; Wong, H.; Kuppusamy, P.; Zweier, J. L.; Ilangovan, G. *Am. J. Physiol. Heart Circ. Physiol.* **2007**, *293*, H3111.
(39) Reeve, J. L.; Szegezdi, E.; Logue, S. E.; Chonghaile, T. N.; O'Brien, T.; Ritter, T.; Samali, A. *J. Cell. Mol. Med.* **2007**, *11*, 509.

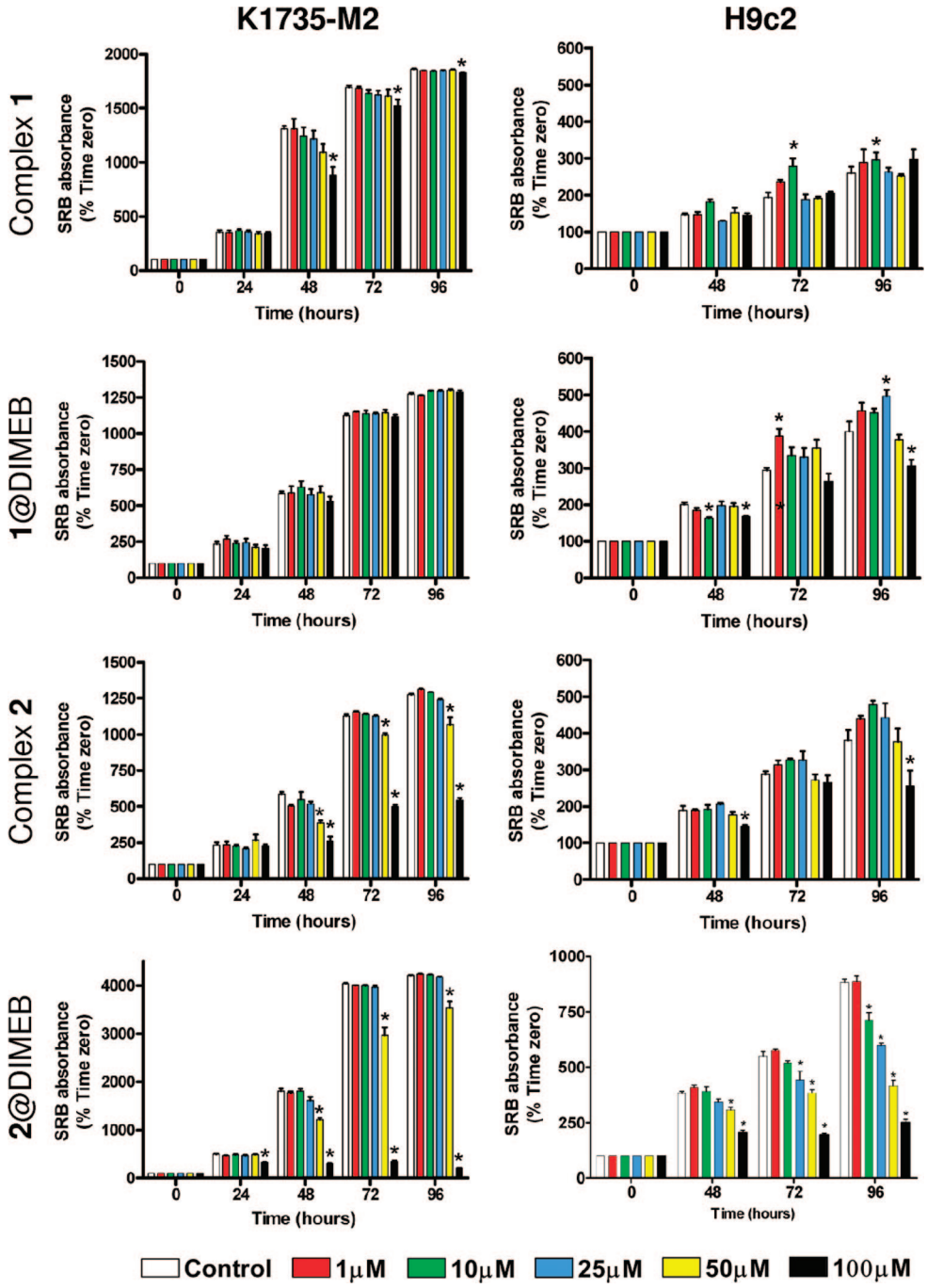


**Figure 7.** Inhibition of cell proliferation by complexes **1**, **2**, **1**@DIMEB, and **2**@DIMEB as measured by the sulforhodamine B dye assay. K1735-M2 and H9c2 cells were seeded as described in the Experimental Section and treated with the different compounds for 24−96 h. Cells in 48-well plates were fixed with 1% acetic acid in methanol. Results are shown as the percentage of time zero, which is an indication of the increase of cell mass, and hence of cell proliferation. Values are means ± SEM of four different experiments. *$p < 0.05$ vs control for the respective time point.

used. Epifluorescence microscopy of K1735-M2 cells, in turn, showed that mitochondrial fragmentation and depolarization occurred at the highest concentrations (50 and 100 $\mu$M) of **2**@DIMEB, although viability was still maintained, indicating that ultracellular alterations may be present even before complete cell death and cell detachment. Despite the fact that the corresponding mechanism is still unknown, these results appear to indicate that mitochondrial alterations take place at an earlier time point than major changes in cell morphology.

The higher cytotoxicity of **2**@DIMEB compared with the free complex was somewhat unexpected, taking into account the structural model derived from the powder XRD data, which shows that the species encapsulated in the host cavity is the tetrafluoroborate anion rather than the half-sandwich $Mo^{II}$ complex cation. This result goes against our previous structural studies of TRIMEB inclusion complexes with the species $CpMo(CO)_3Cl$, $CpFe(CO)_2Cl$, and $Cp_2NbCl_2$, which revealed either partial (involving inclusion of the Cp ligands inside the host cavity) or complete molecular encapsulation.[11g,21a,40] Molecular modeling studies of **2**@DIMEB, including, for example, computation of the molecular lipophilicity patterns,[41] may help to understand the driving forces responsible for the formation of this unusual structure. From the perspective of the organometallic complex cation, **2**@DIMEB is more correctly

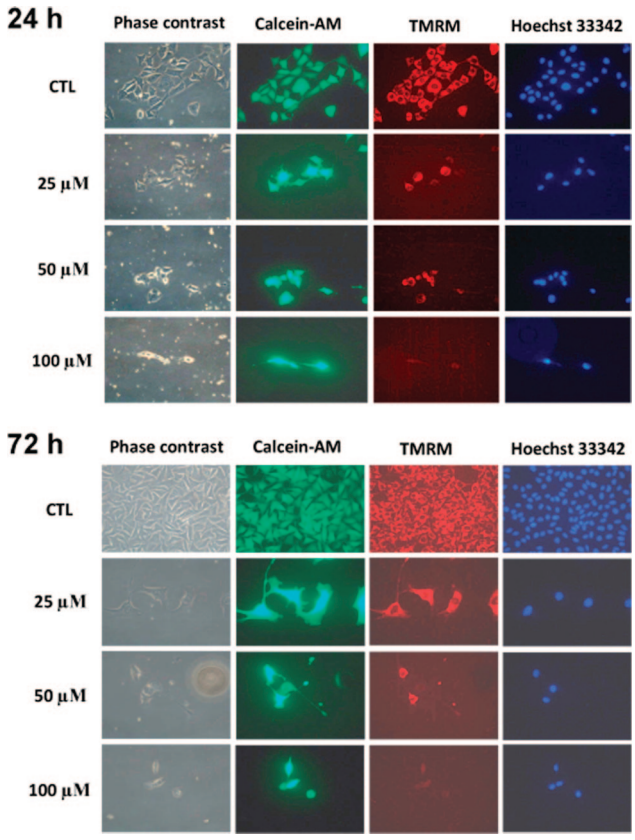


**Figure 8.** Vital imaging of K1735-M2 cells treated with **2**@DIMEB. Cells were incubated with TMRM (red mitochondrial fluorescence, 100 nM), Hoechst 33342 (blue nuclear fluorescence, 1 $\mu$g), and calcein-AM (green cytosolic fluorescence, 300 nM) for 30 min at 37 °C. Experiments were performed for 24 and 72 h of incubation with the compound. Images were obtained with a 40× phase-contrast objective. For 50 and 100 $\mu$M **2**@DIMEB, a clear decrease in the number of cells is visible. Although it appears that the same happens with 25 $\mu$M, the result is due only to the choice of focal plane. For the two higher concentrations, besides the decrease in the number of cells, mitochondrial fragmentation (conversion from long filamentous mitochondria to small round bodies) is also observed, while cells still maintained viability (inclusion of calcein fluorescence). For higher time points (72 h), cells with necrotic phenotype are observed (loss of TMRM and calcein fluorescence) at the highest concentration.

described as a noninclusion complex. The situation may be reversed upon dissolution of **2**@DIMEB; that is, molecular encapsulation of $[CpMo(H_2biim)(CO)_2]^+$ may compete with encapsulation of $BF_4^-$. Even if no inclusion occurs between the cation and DIMEB, we cannot exclude the presence of a noninclusion interaction between the two components able to influence water solubility of the Mo complex,[42] which may in turn be partly responsible for the enhanced cytotoxicity. DIMEB may also function as an absorption enhancer, leading to an increased intracellular accumulation of the drug.[43]

In conclusion, our data indicate that half-sandwich complexes of molybdenum are potentially interesting as anticancer agents and that their bioavailability may be enhanced by combination with cyclodextrins. These findings call for further investigations on the mechanism of action and screening of a broader range of complexes.

## Experimental Section

**General Comments.** All air-sensitive operations were carried out using standard Schlenk techniques under nitrogen. $CH_2Cl_2$ and MeCN were dried over $CaH_2$, distilled under nitrogen, and kept over 3 Å (MeCN) or 4 Å ($CH_2Cl_2$) molecular sieves. Microanalyses for CHN were performed at the University of Aveiro, and Mo was determined by ICP-OES at the Central Laboratory for Analysis (University of Aveiro) by E. Soares. TGA studies were carried out using a Shimadzu TGA-50 system at a heating rate of 5 K $min^{-1}$ under air. Powder XRD data were collected at ambient temperature on an X'Pert MPD Philips diffractometer (Cu Kα X-radiation, $\lambda$ = 1.54060 Å) equipped with an X'Celerator detector, curved graphite-monochromated radiation, and a flat-plate sample holder, in a Bragg−Brentano para-focusing optics configuration (40 kV, 50 mA). Intensity data were collected in continuous scanning mode in the ca. $3° \le 2\theta \le 60°$ angular range. Infrared spectra were recorded on a Unican Mattson Mod 7000 FTIR spectrophotometer. $^{13}C\{^1H\}$ CP/MAS NMR spectra were recorded at 125.72 MHz on a (11.7 T) Bruker Avance 500 spectrometer, with an optimized $\pi/2$ pulse for $^1H$ of 4.5 $\mu$s, 2 ms contact time, a spinning rate of 7 kHz, and 12 s recycle delays. Chemical shifts are quoted in parts per million from tetramethylsilane.

DIMEB was obtained from Fluka and used as received. The complexes $[CpMo(MeCN)_2(CO)_2](BF_4)$ (**1**) and $[CpMo(H_2biim)(CO)_2](BF_4)$ (**2**) were prepared according to literature procedures.[17,44]

**1@DIMEB.** A solution of DIMEB (0.36 g, 0.27 mmol) in acetonitrile was added to a solution of **1** (105 mg, 0.27 mmol) in dry and degassed acetonitrile, and the mixture stirred for 2 h at 40 °C. After cooling to room temperature, the solvent was removed under reduced pressure to obtain a light red microcrystalline solid. Anal. Calcd for $(C_{56}H_{98}O_{35})\cdot(C_{11}H_{11}BF_4MoN_2O_2)\cdot 2H_2O$ (1753.4): C 45.90, H 6.50, N 1.60, Mo 5.47. Found: C 45.96, H 6.56, N 1.10, Mo 5.50. FTIR (KBr, $cm^{-1}$): 3421s, 2929s, 2837m, 1990w ($\nu_{CO}$), 1904m ($\nu_{CO}$), 1643m, 1454m, 1367m, 1332w, 1318sh, 1299w, 1197m, 1159s, 1087vs ($\nu_{BF}$), 1050vs, 1024sh, 967s, 949m, 916m, 857m, 765m, 704m, 610s, 585m, 436w, 373w. $^{13}C\{^1H\}$ CP/MAS NMR: $\delta$ 101.6 (DIMEB, C1), 82.7 (DIMEB, C2,4), 70.5 (DIMEB, C3,5,6), 59.8 (DIMEB, O-Me).

**2@DIMEB.** A solution of DIMEB (0.15 g, 0.11 mmol) in dichloromethane was added to a solution of **2** (49 mg, 0.11 mmol) in dichloromethane and the mixture stirred for 2 h at 40 °C. After cooling to room temperature, the solvent was removed under reduced pressure to obtain a light brown microcrystalline solid. Anal. Calcd for $(C_{56}H_{98}O_{35})\cdot(C_{13}H_{11}BF_4MoN_4O_2)\cdot 3H_2O$ (1823.4): C 45.45, H 6.36, N 3.07, Mo 5.26. Found: C 45.43, H 6.14, N 3.50, Mo 5.21. FTIR (KBr, $cm^{-1}$): 3423s, 2927s, 2840m, 2030m, 1976s ($\nu_{CO}$), 1890s ($\nu_{CO}$), 1731m, 1646m, 1540m, 1461m, 1429m, 1408w, 1371m, 1332w, 1297m, 1260m, 1197m, 1159s, 1087vs ($\nu_{BF}$), 1051vs, 966s, 916m, 863m, 826w, 757m, 736m, 704m, 673w, 609s, 573m, 440m, 376w. $^{13}C\{^1H\}$ CP/MAS NMR: $\delta$ 134.7, 122.5 ($H_2biim$), 102.2 (DIMEB, C1), 96.9 (Cp), 82.9 (DIMEB, C2,4), 71.1 (DIMEB, C3,5,6), 60.4, 60.0, 59.6 (DIMEB, O-Me).

**Cell Culture.** K1735-M2 mouse melanoma cells (kindly provided by Dr. Lillian Repesh, Department of Anatomy, Microbiology and Pathology, University of Minnesota, Medical School, Duluth, MN) were grown in Dulbecco's modified Eagle's medium (DMEM; Gibco, Grand Island, NY) supplemented with 1.5 g/L sodium bicarbonate and 10% fetal clone III (FC3; HyClone, Logan, UT)

(40) Balula, S. S.; Coelho, A. C.; Braga, S. S.; Hazell, A.; Valente, A. A.; Pillinger, M.; Seixas, J. D.; Romão, C. C.; Gonçalves, I. S. *Organometallics* **2007**, *26*, 6857.
(41) (a) Lichtenthaler, F. W.; Immel, S. *Starch/Stärke* **1996**, *48*, 145. (b) Immel, S.; Lichtenthaler, F. W. *Starch/Stärke* **1996**, *48*, 225.
(42) Loftsson, T.; Másson, M.; Brewster, M. E. *J. Pharm. Sci.* **2004**, *93*, 1091.
(43) Upadhyay, A. K.; Singh, S.; Chhipa, R. R.; Vijayakumar, M. V.; Ajay, A. K.; Bhat, M. K. *Toxicol. Appl. Pharmacol.* **2006**, *216*, 177.
(44) Drew, M. G. B.; Félix, V.; Gonçalves, I. S.; Kühn, F. E.; Lopes, A. D.; Romão, C. C. *Polyhedron* **1998**, *17*, 1091.

in a 5% $CO_2$ atmosphere at 37 °C. Cells were passaged by trypsinization using standard methods; all experiments were performed in cells seeded from cultures in log-phase growth. The H9c2 cell line, originally derived from embryonic rat heart tissue using selective serial passages,[45] was purchased from America Tissue Type Collection (Manassas, VA; catalog # CRL-1446). Cells were cultured in DMEM supplemented with 1.5 g/L sodium bicarbonate, 10% fetal bovine serum, 100 U/mL penicillin, and 100 $\mu$g/mL streptomycin in 75 $cm^2$ tissue culture flasks at 37 °C in a humidified atmosphere of 5% $CO_2$. Cells were fed every 2−3 days and subcultured once they reached 70−80% confluence.

**Cell Proliferation Measurements.** Sulforhodamine B assays[46] were conducted to measure the effects of the compounds under study on the proliferation of K1735-M2 cells, essentially as described by Holy et al.[47] H9c2 and K1735-M2 cells were seeded at a concentration of $1 \times 10^4$ cells/mL in 48-well plates and allowed to recover for 1 day prior to drug addition. Vehicle controls were also performed. After sulforhodamine labeling in acidic buffer, absorbance was measured in a spectrophotometer at 540 nm; the amount of dye released is proportional to the number of cells present in the dish and is a reliable indicator of cell proliferation. Values were measured in terms of percentage of time zero (i.e., the cell mass before drug or vehicle treatment) and compared with the control for the respective time point.

**Epifluorescence Imaging of K1735-M2 Cells.** Cells were seeded in glass coverslips at a concentration of $1 \times 10^4$ cells/mL. Cells were allowed to attach for 24 h and then treated with **2**@DIMEB or with the vehicle (DMSO) for the desired time. Before the drug exposure time ended, cells were incubated with TMRM (100 nM), Hoechst 33342 (1 $\mu$g), and calcein-AM (300 nM) diluted in standard calcium-supplemented Krebs buffer for 30 min at 37 °C in the dark. Before collecting the images, the media with the fluorescent probes was replaced by fresh Krebs media without probe addition. Images were collected using a 40× objective in an epifluorescence Leica DM 4000B.

**Statistics.** Data are represented as means ± SEM and compared by using ANOVA followed by the Dunnett's post-test. A value of $p < 0.05$ was considered significant. Analyses were conducted by using GraphPad Prism 4.0 (GraphPad Software).

**Acknowledgment.** We are grateful to the FCT, POCI 2010, OE, and FEDER for funding (Project POCI/QUI/56109/2004). We also wish to acknowledge Prof. João Rocha for access to research facilities and Paula Esculcas for assistance in the NMR experiments. We are grateful to Celeste Azevedo for carrying out the TGA experiments and to Rosário Soares for collection of the powder diffraction data.

**Supporting Information Available:** Le Bail whole-powder-diffraction-pattern profile fitting in the orthorhombic $P2_12_12_1$ space group, table with the fractional atomic coordinates (as supplied by FOX), and CIF file with the optimized structural model of **2**@DIMEB. This material is available free of charge via the Internet at http://pubs.acs.org.

OM800413W

(45) Kimes, B. W.; Brandt, B. L. *Exp. Cell Res.* **1976**, *98*, 367.
(46) Skehan, P.; Storeng, R.; Scudiero, D.; Monks, A.; McMahan, J.; Vistica, D.; Warren, J. T.; Bokesch, H.; Kenny, S.; Boyd, M. R. *J. Natl. Cancer Inst.* **1990**, *82*, 1107.
(47) Holy, J.; Lamont, G.; Perkins, E. *BMC Cell Biol.* **2006**, *7*, 13.